Visualization of working electrode reactivity from an electrochromic counter electrode

Qiao Liu, Mariela Alicia Brites Helú, Alain Walcarius, Liang Liu

Visualization of working electrode reactivity from an electrochromic counter electrode

Qiao Liu, Mariela Alicia Brites Helú, Alain Walcarius, Liang Liu*

Université de Lorraine, CNRS, Laboratoire de Chimie Physique et Microbiologie pour les Matériaux et l'Environnement (LCPME), F-54000 Nancy, France ;

**Email : liang.liu@cnrs.fr; liang.liu@univ-lorraine.fr*

Abstract

Understanding local electrochemical reactivity of surfaces is crucial for electrode design and applications at device level, in the fields of energy storage, biosensing, or electrocatalysis. In this work, we attempt to optically map the local electrochemical reactivity of surfaces not by "looking" at the working electrode (WE), but by measuring optical change of the counter electrode (CE). The concept is based on an electrochromic CE that changes color with electron transfer accompanying ion intercalation. As the CE is placed in parallel with the WE and maintains a micrometer range distance, the optical transmittance of CE reduces locally at positions corresponding to the active area of WE when applying a suitable anodic potential. The change can be captured dynamically in the form of video, which offers information on the transient behavior of the system. The spatial resolution of CE imaging increases as the distance between WE and CE decreases, likely due to the de-homogenization of current distribution on CE. The reported method offers a label-free alternative for measuring "invisible" electrochemical reactions, that is to say, does not require to modify neither the WE nor the electrolyte.

Keywords: electro-optical imaging; electrochromic counter electrode; WO_3; local electrochemical reactivity; ensembles/arrays of ultramicroelectrodes.

1. Introduction

Measuring local electrochemical reactivity of electrodes is highly important for fundamental understanding of the materials as well as engineering of electrochemical devices [1–5]. This is usually achieved by scanning electrochemical probe techniques, such as scanning electrochemical microscopy (SECM) and scanning electrochemical cell microscopy (SECCM) [6,7]. With the recent development of nanoelectrodes and nano-capillaries, the spatial resolution of SECM and SECCM could reach tens of nanometers. However, to generate a map of electrochemical signals, the probe has to scan over the sample surface, which is intrinsically slow. It may take from minutes to hours, making it impossible to map transient electrochemical processes at high temporal resolution.

On the other hand, optical imaging is much faster with modern cameras. Even without special camera, it typically takes tens of milliseconds to acquire a static image, which is already several orders of magnitude less as compared with scanning probe techniques. Moreover, one may easily achieve good spatial resolution up to the diffraction limit of the light (<1 μm) without special optics. Thus, optical imaging is ideal for high throughput measurements and is widely used in industry [8,9].

Nevertheless, most of the electrochemical reactions cannot be directly “seen”. It is essential to quantitatively convert the electrochemical reactions to measurable optical signals. For example, Tao and co-workers have developed electrochemical surface plasmon resonance microscopy (SPRM), where they derived quantitative links between

SPR intensity and local electrochemical signals, *i.e.* current density, double-layer capacitance and charge transfer resistance [10,11]. The technique has been used to monitor the electrocatalytical activity of single nanoparticles in real-time [12–15]. Note that SPRM is usually performed on thin gold film electrodes for the sake of getting significant SPR signals. This would limit practical applications due to the potential interference from the oxidation of gold under anodic bias and/or the instability of gold films in acidic media. Another strategy is to "look" at reactions that involve photo-responsive molecules, such as electrochemical fluorescent microscopy or electrochemiluminescence microscopy [9,16]. The former is based on the electrochemical production of molecules that can either excite or quench fluorescence, and the latter is based on the excitation of luminophore that emits light. In both cases, the optical signal intensity is linked to the quantity of electrochemically generated photo-responsive or photo-active species, which reflect the electrochemical reaction kinetics on the working electrode (WE). Yet, they are limited to a few special reactions. To target more general "invisible" reactions, one needs to add photo-responsive molecules (or their precursors) or luminophore and design special reaction routes [17,18]. This would inevitably change the target system of interest. Another strategy is to monitor the change of WE and/or the electrolyte in Raman [19] or IR spectromicroscopy [20,21]. The reaction kinetics is then analyzed through the variation of the concentration of intermediates or the intensity of chemical bonds. The method is highly informative, but compromise has to be made for gaining time resolution in mapping, which is usually achieved by measuring at a single wavelength or wavenumber. This requires careful selection of experimental conditions and makes quantification only reliable for very well separated peaks. From the optical

measurement aspect, all the approaches above focus on the WE sample, that is, capturing the image by directly “looking” at the optical change of WE as a result of electrochemical reactions.

In an electroanalytical system, it is natural for electrochemists to study the interface between WE and the electrolyte, whereas another interface of counter electrode (CE) is often neglected. While CE is usually designed not to interfere with WE, in some cases it may also purposely regulate the electric field distribution by controlling its size and position relative to the WE [19,20]. A typical example is direct mode SECM, where a microelectrode serving as CE is positioned close to a macro-sized WE sample. This spatially localizes the electrochemical reactions in the vicinity under the micro-CE by regulating the current flux. It is widely used for patterning surfaces by local electrochemical deposition or etching, and the shape of pattern almost replicates that of the micro-CE when the distance between the sample (WE) and the microelectrode (CE) is comparable to the radius of the micro-CE [21]. Similarly, by placing a planar CE in parallel with a planar WE at short distance, the current distribution on WE which reflects the local electrochemical reactivity, would also cause inhomogeneous current distribution on CE. Owen group [22] reported that the color of WO_3 electrochromic CE locally changes following the exposed area of WE, and the absorption corresponds to the catalytic reactivity of the WE. They used WE array, in which each electrode had 1 mm diameter and the gap was 3 mm between adjacent electrodes.

In this work, we attempt to extend the concept of visualizing electrochemical reactions on WE indirectly through the optical change of the CE. The experimental configuration consists of a planar WE (interdigitated electrode, microelectrode array, and micro-Au disk sputtered on ITO), a WO_3-coated ITO as CE, and pure water as electrolyte. The

two electrodes are separated by a PTFE spacer to control the distance. This would get rid of potential interference from the inhomogeneity of filter paper used in literature [22]. The two-electrode electrochemical cell is fixed on an optical microscope, where a complementary metal oxide semiconductor (CMOS) camera is synchronized with potentiostat for capturing the dynamic color change of the CE. The latter is observed to reflect the electrochemical reactivity distribution of WE.

2. Experimental section

2.1 Materials and electrode preparation

Hydrogen peroxide (H_2O_2, 30%), ammonium hydroxide (NH_4OH, 25%), tungsten powder (W, 99.99%), and platinum on carbon powder (Pt/C, 10 wt.% loading) were purchased from Sigma-Aldrich. All reagents were of analytical grade and used without further purification. Deionized water obtained from a Millipore water purification system (≥18 MΩ·cm, 25 °C, Milli-Q, Millipore Co.) was used in all experiments.

The WO_3 electrochromic CE was prepared by electrodeposition on ITO (Thickness: 0.5 mm, 10 Ω/sq, area: 15 × 15 mm^2, SPI Supplies, France) from peroxo-tungstic acid (PTA) solution. The latter was prepared by dissolution of 1.8 g of W metallic powder in 20 ml of H_2O_2 and 20 mL of deionized water [23]. The mixture was constantly stirred for 24 h in a cold bath (between 0 and 10 °C). Then, 0.05 g of Pt/C powder was added into the colorless solution to catalyze the decomposition of excess H_2O_2 under string until obtaining a yellow-colored solution. Next, the obtained PTA solution was further centrifuged at 7000 rpm for 8 min in order to remove the precipitate, while the supernatant was recovered and kept in the refrigerator for further use. The electrodeposition was carried out in a conventional three-electrode system, with ITO as

WE, an Ag/AgCl commercial RE (in saturated KCl), and a Pt wire as CE. Before electrodeposition, the ITO surface was cleaned by sonication in acetone, ethanol, $H_2O_2/NH_3{\cdot}H_2O$ (2:1 *vol.* ratio) and water. The WO_3 film was electrodeposited by scanning cyclic voltammetry between 0 and -0.6 V (*vs.* Ag/AgCl in saturated KCl) at a scan rate of 2 mV/s for 10 cycles. After electrodeposition, the film was rinsed with water and dried in air. The as-prepared WO_3 film showed dark blue color due to the electrochemical reduction, but it was rapidly oxidized and bleached after a few seconds of exposure in air [24]. The WO_3-coated ITO was stored under ambient condition for use.

The WEs studied include interdigitated Au electrodes (200 µm band with 200 µm gap, Metrohm, denoted as Au-IDE), Au-disk array on ITO and Au microelectrode array. The Au-disk array was deposited by sputtering Au on masked ITO for 120 s at 35 mA current to achieve thickness of *ca.* 60 nm (Quorum sputter coater, Q150 TS). The mask was printed on SLA 3D printer (Asiga) with 200 µm diameter holes, and was removed after sputtering. The Au microelectrode array was prepared by sealing Au wires (25 µm diameter, 99.9%, ChemPur, Germany) in UV-cured resin. First, the structural body of the array with holes of *ca.* 150 µm diameter was 3D printed from UV DLP resin. The Au wires were then inserted in the holes under stereomicroscope, and the holes were closed by filling the same resin as that for printing. Afterwards, the structure was cured in UV for at least 1 hour. The electrical connections of Au wires was made by attaching to a Cu sheet with silver epoxy (M.G. Chemicals, UK). The final step was to polish the Au microelectrode array on 0.1 µm abrasive disc (Buehler, USA) to ensure a smooth surface with Au wires well exposed.

2.2 Electrochemical cell assembly and measurements with optical imaging

The electrochemical cell was assembled in a sandwich configuration by pressing the WE, the spacer and the WO_3/ITO CE together. The electrodes were fixed in a 3D printed frame by two magnets (**Fig. 1A**). Polytetrafluoroethylene (PTFE) spacers of 0.005 − 0.1 mm thickness (Goodfellow, UK) were used to separate WE from CE and control the distance between them. A square hole of 2 mm × 2 mm was made for filling the deionized water electrolyte. After assembly, the electrochemical cell was placed under optical microscope for imaging.

The optical imaging system is illustrated in **Fig. 1B.** A red LED of 623 nm wavelength was used as light source (Thorlabs). The objectives were 4× (NA = 0.10) and 10× (NA = 0.25) from Olympus, Japan. The imaging was carried out by a CMOS camera (Thorlabs).

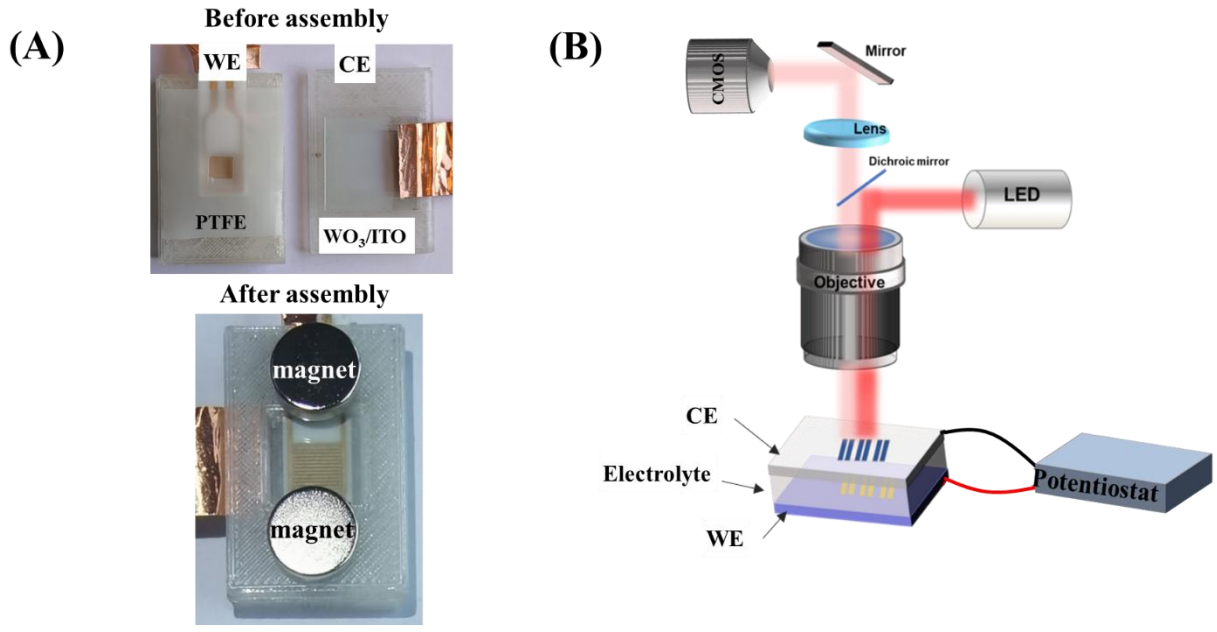

Fig. 1. (A) The photos of cell. (B) Schematic diagram of the imaging system.

Electrochemical and optical measurements were synchronized for visualizing the CE color change upon applying voltage between WE and CE. The voltage was controlled by a potentiostat (PalmSens 4, Netherland). Synchronization between the potentiostat and the CMOS camera was achieved by an Arduino Uno R3 microcontroller. The latter is programmed to generate a square wave once receiving a trigger signal. When an electrochemical measurement started, a trigger was sent to Arduino, marking the starting time. The consequently generated square wave triggers the image capturing at desired time intervals by the CMOS camera. The exposure time of camera was 8 ms for each image. In this way, the optical images could precisely reflect the transient behavior of the electrochemical system. The images were post-analyzed by ImageJ software.

3. Results and discussion

The reactions occurring at a counter electrode cannot be neglected when the CE is placed close to WE, and this will affect the electrochemical response of the cell. Thus, for analyzing such system, one needs to consider the electrochemical reactions on both WE and CE. Moreover, when the WE and CE are different, either in size or in reactivity, the current distribution shall also be taken into consideration. For example, in direct mode SECM, the microelectrode determines the current distribution on the large-scale substrate and localizes the reactions [21]. Another example is Pt electrocatalyst on carbon substrate. The Pt may locally catalyze the electrochemical oxidation of methanol, yielding higher current density which triggers deeper color change of an electrochromic CE [22].

Taking advantage of the interactions between WE and CE at short distance, we demonstrate an example where an Au-IDE is placed in parallel with a WO_3

electrochromic CE. Deionized water without added electrolyte is used as the solution, with the consideration of having high resistance and relatively simple reactions. By applying an anodic bias on WE, H_2O is oxidized on WE and WO_3 is reduced on CE. The scheme is shown in **Fig. 2A**. The reactions are depicted as follows:

WE: $2H_2O \rightarrow O_2 + 4H^+ + 4e^-$

CE: $WO_3 + xH^+ + xe^- \rightarrow H_xWO_3$

The reduced form H_xWO_3 is blue-colored and can be visualized by naked eyes or under optical microscope. **Fig. 2B** illustrates the color change of the system during a linear sweep voltammetry scan. At 1.3 V, the current is very low (*ca.* 3.85 μA) and the WO_3 CE stays transparent. This suggests that the reactions on both WE and CE are negligible. As the applied voltage increases beyond 1.5 V, the current sharply increases and the WO_3 CE starts to turn blue. Moreover, the blue strips on CE fall almost exactly above the Au strips on WE. This indicates that the current distribution on CE follows that on WE. In another word, the shape of WE can be "projected" to CE.

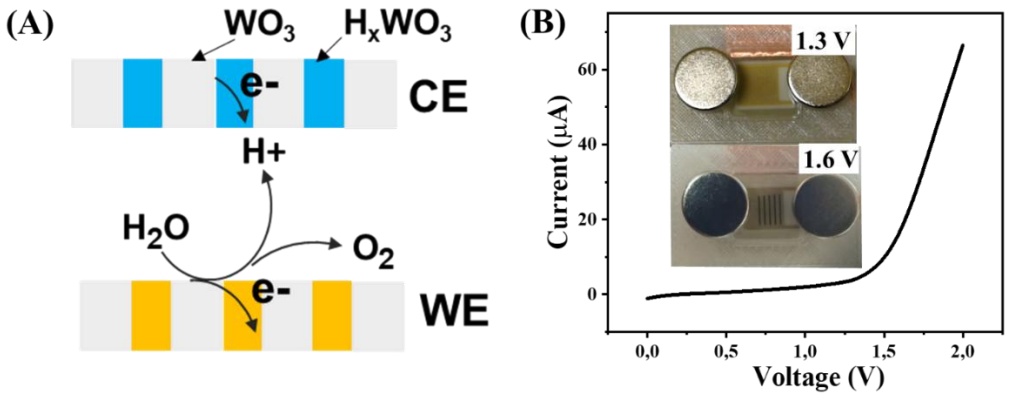

Fig. 2. (A) Schematic diagram of the reaction mechanism of Au-IDE as WE (yellow) and WO_3 film on ITO as CE (localized oxidation depicted in blue). (B) Linear sweep voltammetry of Au-IDE *vs.* WO_3/ITO CE from 0 to 2.0 V at a scan rate of 0.05 V/s (Inset: photos of CE at 1.3 and 1.6 V).

The color change of CE was quantitatively measured under optical microscope with a CMOS camera. The electrochemical cell was fixed under optical microscope with the optical focus on the WE. When scanning the voltage from 0 to 2 V (WE *vs.* CE), images were taken at various moments, which correspond to different applied voltage thanks to the synchronization. According to the scheme in **Fig. 1B**, the light irradiates the WE surface and reflects back to the camera. In the optical pathway, it goes through CE and electrolyte for two times (incite and reflected light). Assuming that the optical properties of the WE and the electrolyte do not change during the experiment, the light intensity captured by the camera reflects only the electrochromic effect of the CE. The transmittance of CE can thus be derived by dividing the gray value of the colored state by that of the bleached state. In this work, the image taken at 0 V was considered as bleached state for the normalization of gray values. It is seen that the normalized image at 1.3 V shows no strip (**Fig. 3A**), which agrees well with no visible color change in **Fig. 2B**. As the applied voltage increases to 1.6 V, the strips start to appear (**Fig. 3B**). This suggests local coloration of the CE in the areas above the Au strips, which differs from those between them. As the applied voltage further increases to 1.9 V, the contrast between colored strips and the gaps becomes higher (**Fig. 3C**). **Fig. 3D** shows the variation of normalized gray values across the strips (in horizontal direction in the images). The normalized gray values of the areas above Au strips decrease as the applied voltage increases, indicating that the absorption of WO_3 CE increases. Although the normalized gray values of the areas above gaps between Au strips also decrease obviously after 1.6 V, it could be neglected compared to the normalized gray values of the strips. Moreover, the width of the colored strips is almost identical to that of the Au

interdigitated electrodes. This indicate that one may identify conductive areas of WE from the local color change of electrochromic CE.

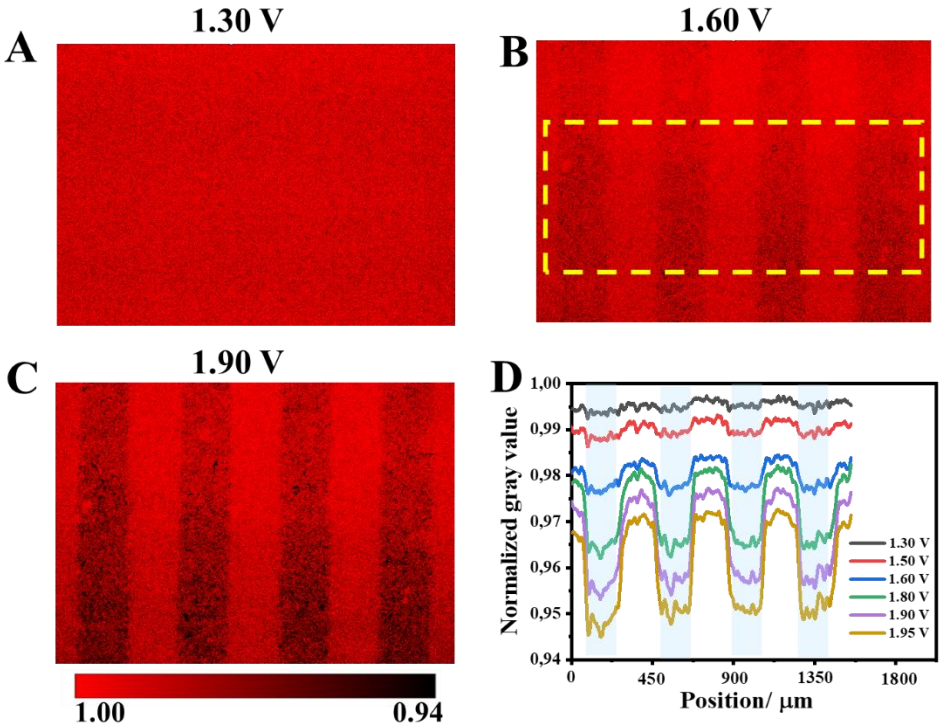

Fig. 3. The images in normalized gray value for Au-IDE WE *vs.* WO_3/ITO CE system at voltage of 1.30 (A), 1.60 (B) and 1.90 V (C). Scale bar (white): 200 μm. (D) The average normalized gray values across the strips and gaps in the yellow dotted frame in Fig. 3B at different applied voltage.

The color change of CE was also measured as a function of time by applying a constant voltage between WE and CE. **Fig. 4** shows the images captured at 1, 5 and 15 s when applying 1.9 V on WE *vs.* CE. It is seen that the normalized gray value of the colored strip, which corresponds to the Au strip on WE, gradually decreases with time. Moreover, the areas above the gap between Au strips also start to be colored after *ca.* 5 s. Considering that the distance between WE and CE is 25 μm, even 1 s would be sufficient for the H^+ generated on WE diffusing to the CE. Thus, the enhancement in

coloration with time is likely related to the kinetics of WO_3 coloration on CE, which is known to be relatively slow in the order of a few seconds [25]. However, as the coloration of WO_3 is driven by intercalation of H^+ in the film, the lateral propagation of H^+ may result in the expansion of colored strips at long time. This may explain the decrease in the normalized gray values, or the increase in coloration, of the gap with time (**Fig. 4C**).

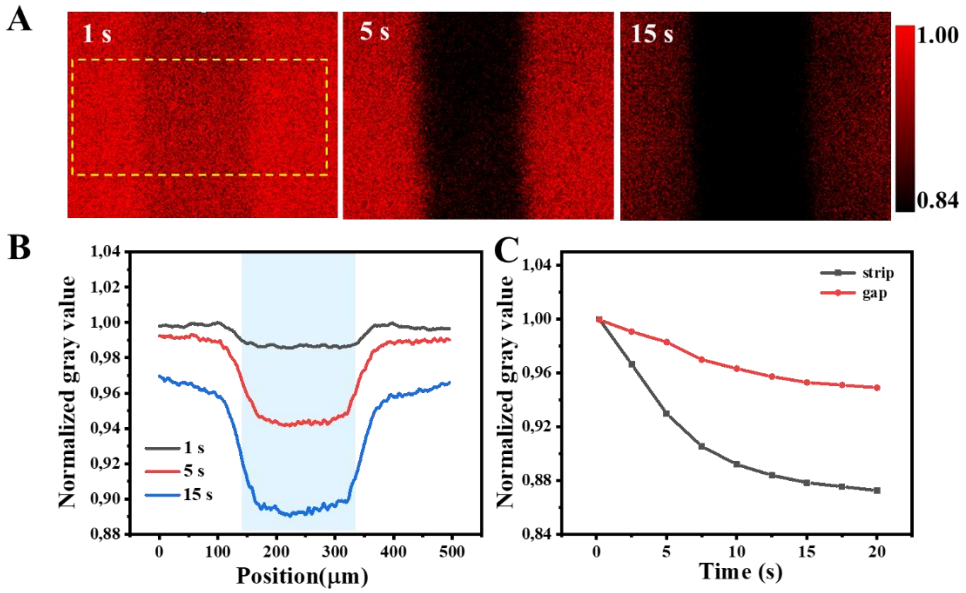

Fig. 4. Au-IDE WE *vs.* WO_3/ITO CE system at 1.9 V with different time: (A) The normalized gray value images; (B) The average normalized gray value across the region in the yellow dotted frame in Fig. 4A. (C) Normalized gray value at the strip and the gap as a function of time.

As the local color change on CE is determined by the current distribution in the electrochemical cell, the distance between WE and CE is likely to play an important role. **Fig. 5** shows the images taken at 1.5 V for 5 s, with Au-IDE as WE and WO_3/ITO as CE, when using a spacer of different thickness. It can be seen that with a distance of

0.2 mm from WE and CE, there is no visible color strip on CE (**Fig. 5A**), while reducing the thickness of the PTFE spacer, strip starts to appear (**Fig. 5B**). Moreover, the current response decreases as the WE-CE distance increases (**Fig. S1**), which could be explained by the resistivity of the electrolyte as well as the longer distance for mass transport of H^+. The normalized gray values of the strip and the gap are almost the same at WE-CE distance of 0.2 mm (**Fig. 5C**), meaning that the color change of CE is insignificant. When the distance is less than 0.05 mm, the normalized gray value of the strip becomes significantly lower than that of the gap. This suggests that WE and CE being close is more favorable for projecting the current distribution on WE to CE.

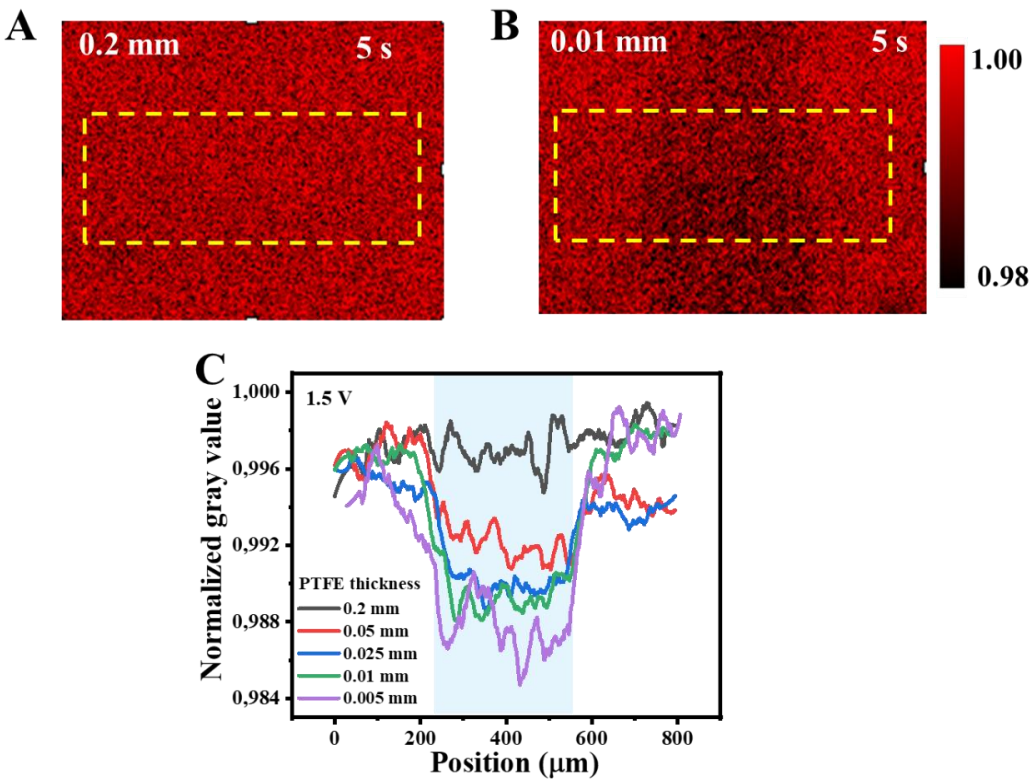

Fig. 5. The normalized gray value images of Au-IDE WE *vs.* WO_3/ITO CE system at 1.5 V for 5 s, with WE-CE distance at 0.2 (A) and 0.01 mm (B); The average normalized gray value of the strips across the regions in the yellow dotted frames with different thickness of the PTFE spacer.

The imaging of CE is further challenged with higher spatial resolution using Au microelectrode array as WE. **Fig. 6A** shows the optical image of the microelectrode array, where each Au microelectrode has a diameter of 25 μm and the gap between adjacent electrodes varies from 20 to 250 μm. By scanning the voltage between WE and CE from 0 to 2 V with 10 μm WE-CE distance, the current shows a sharp increase at *ca.* 1.5 V, which corresponds to the onset of electrochemical oxidation of water (**Fig. S2**). Meanwhile, the color above the areas of Au microelectrodes also starts to change, and the coloration becomes more significant as the applied voltage further increases (**Fig. 6B**). Note that electrodes 7 and 8, which are located very close to each other (20 μm), become less distinguishable at high voltage (**Fig. 6C**). This lateral propagation of color is consistent with the observations on Au-IDE. It suggests that the distance between adjacent active spots on WE would affect the electrochromic imaging from CE. Experimentally, by controlling proper voltage, it is still possible to visualize 25 μm active electrodes with an insulating gap of *ca.* 20 μm.

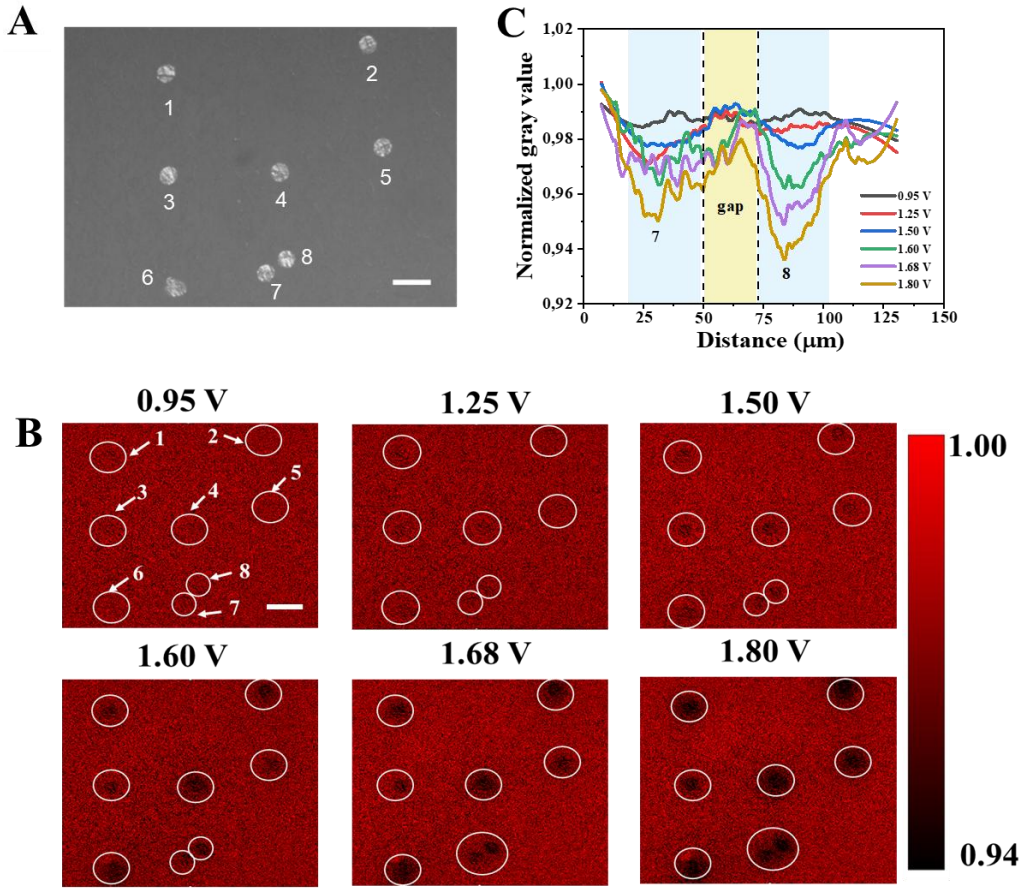

Fig. 6. Au microelectrode array WE *vs.* WO_3/ITO CE: (A) Optical microscopy image; (B) Normalized gray value images at different applied voltage; (C) Normalized gray value of the region 7, 8, and the gap. Scale bar (white): 50 μm.

The examples above, *i.e.* Au-IDE and Au microelectrode array, are partially conductive. They could be considered as extreme cases where the WE has high contrast between reactive (Au electrodes) and non-reactive (insulator) areas. Yet a question arises: Does the local coloration originate from the difference in the electrical conductivity or the electrochemical reactivity? To address this, we demonstrate that the visualization from CE could also be extended to samples with different conductive materials. Optical imaging was recorded while scanning voltage of an Au-sputtered ITO electrode (**Fig.**

7A) against a WO_3/ITO CE with 25 μm distance and H_2O as electrolyte (**Fig. 7B**). After normalizing images with that taken at open circuit voltage (*ca.* 0.005 V), the micro-disks are almost invisible on the CE when the applied voltage is lower than *ca.* 1.0 V (**Fig. 7C**). When the voltage rises to *ca.* 1.1-1.3 V, the micro-disks become distinguishable. It is interesting to see that the edges of the disks have lower normalized gray values than the centers and the ITO gaps (**Fig. 7D**). This will be discussed later. As the voltage increases to higher than 1.4 V, the color change of CE over the disks is more significant with a decrease in normalized gray value, and it also becomes more uniform. This suggests that the current passing through Au is higher than that through ITO, which could be related to their different electrocatalytic reactivity for the oxidation of water. However, when the voltage is further increased to 1.8 V, the ITO gaps between Au disks also start to change color. This could be attributed to two possible effects: one is the lateral charge propagation due to higher current and lateral mass transport of H^+, which is similar as observed from partially conductive samples (**Fig. 3** and **4**); the other is the reduced contrast in electrocatalytic reactivity between Au and ITO, as ITO could also catalyze water oxidation at high potentials.

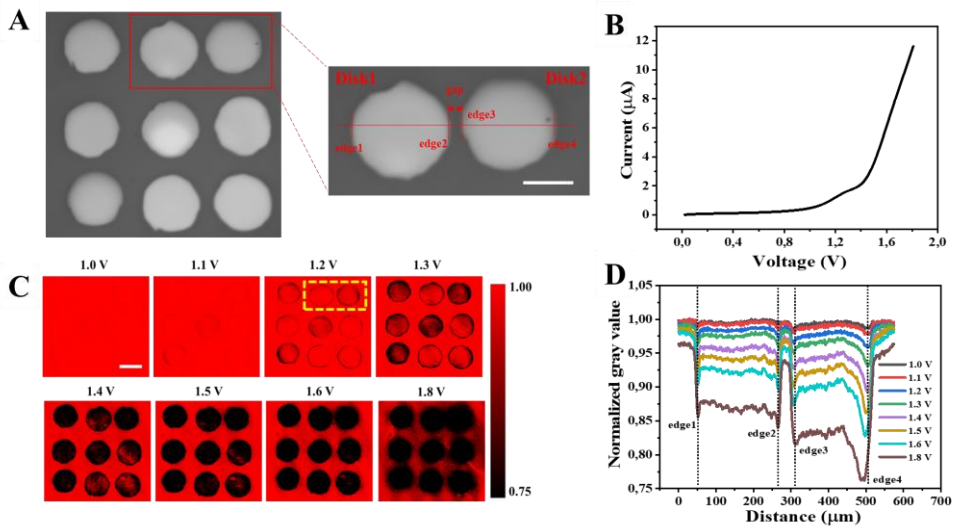

Fig. 7. Au disks sputtered on ITO as WE *vs.* WO_3/ITO CE: (A) Optical microscopy image. Scale bar (white): 100 μm; (B) Linear sweep voltammetry from 0 to 2.0 V at a scan rate of 0.05 V/s; (C) Normalized gray value images at increasing voltage on WE. Scale bar (white): 200 μm; (D) Average normalized gray value of the two micro-disks on CE (the yellow dotted frame in Fig. 7C). The edges (1−4) correspond to the edges of the two micro-Au disk on the WE in Fig. 7A.

Throughout the work, the light intensity (gray value) captured by the camera is systematically normalized with that measured from WO_3 CE at bleaching state. The normalized gray value can be linked to the transmittance of the WO_3 CE only under pre-assumptions that the transmittance of water and the reflectance of WE remain unchanged during the measurement. The former is acceptable when the generation of gas bubbles is insignificant. This is why we did not test higher voltage. However, the latter could be questionable as the optical properties of Au surface were reported to vary under applied potential [26]. **Fig. 8** shows a control experiment for **Fig. 7**. The WO_3/ITO CE was replaced by bare ITO, which is considered non-electrochromic before its irreversible reduction. As compared to **Fig. 7B**, it is seen that the current is much lower at the same applied voltage, and the oxidation wave between 1.0 and 1.4 V disappears (**Fig. 8A**). This could be explained by the removal of redox reactions of WO_3. The optical images with normalized gray values look very similar for different applied voltage. Yet, the edges of Au disks could still be distinguished especially when the voltage is high, although it has much less contrast to the Au disk and the gap as compared with **Fig. 7**. One should be very careful in interpreting this edge effect. On one hand, the optical pathway at the junction between Au and ITO is very complex due to their different reflectivity. This might cause some artifacts in imaging. On the other hand, it could also be electrochemically much more active due to Schottky effect [27].

This would result in an improvement in catalyzing water oxidation, and could explain the appearance of normalized gray value change at edges prior to the center of Au disks in **Fig. 7**. Another control experiment was made with a homogeneous Au electrode as WE and bare ITO as CE, and the results confirmed that the change in the reflectivity of Au was negligible, which fulfilled the pre-assumption (**Fig. S3**).

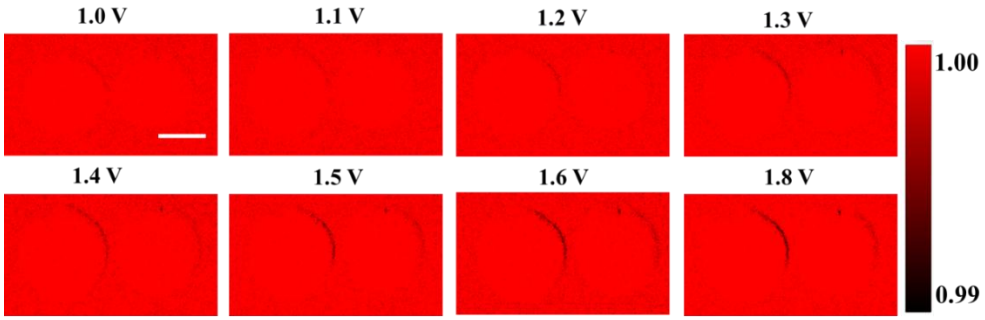

Fig. 8. The control experiment with Au disks sputtered on ITO as WE *vs.* bare ITO CE: (A) linear scan voltammetry at scan rate of 0.05 V/s; (B) Normalized gray value images with increasing voltage. Scale bar (white): 100 μm.

The experimental results above clearly demonstrate the link between CE color change and the reactivity of the WE. It arises from the inhomogeneous current distribution in the electrochemical cell. This is counter intuitive to usual principles of electrochemical cell design. The most important is to have the CE very close to WE for "projecting" the pattern. It may restrict the cell design, as the roughness of the electrodes shall be considered in the order of a few microns. Besides, high resistance of electrolyte is preferred to inhibit lateral dispersion of current in the solution, and facilitate the migration of intercalating ions such as H^+. This is why we used pure water without adding supporting electrolyte. Note that due to the small WE-CE distance, one could still work with usual cell voltage (<2 V) as the cell resistance is still relatively low.

The electrochromic reaction of WO_3 CE requires the intercalation of H^+ (**Fig. 2A**). A question then arises: Can pure water provide enough H^+ for the color change? With 10^{-7} mol/L concentration in pure water, it is clearly not enough for inducing the clear color change observed in this work. However, one should consider the oxidation of water on WE that generates H^+. The H^+ generated on WE can easily reach CE with mass transport since the two electrodes are positioned close to each other. It is similar as generation-collection mode of SECM [28]. Note that the electrolyte is weakly supported, migration could also play an important role. Considering that H^+ is positively charged, migration facilitates its transfer from WE to CE when applying positive bias on WE. This is beneficial for localizing the current distribution on CE.

The direct projection of WE reactivity to CE color change is only an ideal case. The lateral charge propagation on CE is unavoidable, and even a more general situation. It could occur when applying high voltage (**Fig. 3**), or applying voltage for long time (**Fig. 4**), or having two reactive spots close to each other on WE (**Fig. 6**). While the former two could still be optimized with experimental conditions, the latter depends on the property of the sample thus may limit the application of the method. A better way would be the quantitative analysis of the reactivity of WE from the optical signals on CE by modeling. This is beyond the scope of the present work, but let's discuss briefly some prerequisites. The model should consider the electrochemical reaction kinetics on both WE and CE, the mass transport of species in the electrolyte including diffusion and migration, and the lateral boundary conditions. Mathematically, two types of lateral boundary conditions are convenient to work with. One is symmetry or no-flux, where the lateral flux of species at boundary is zero. This is applicable for the cell boundary regulated by PTFE spacer, and also for highly symmetrical systems like Au-IDE.

Another type is semi-infinite diffusion, where the concentration of species always equals to the initial condition (bulk) at the boundary. This is applicable for studying reactive sites that are well apart, with an inert background, such as points 1-6 in **Fig. 6**.

From the experimental aspect, several improvements can also be foreseen. The optical signal acquisition could be carried out at multiple wavelengths to improve the sensitivity in capturing the electrochromic change of CE. The electrochromic material for CE could also be optimized for higher color switching speed. This could eliminate the kinetic effect of CE by replacing with Nernst boundary condition, which would greatly ease the analysis of transient behavior of WE. Besides oxidation reactions that can be "seen" through cathodically colored electrochromic films, reduction reactions can also be studied with anodically colored electrochromic materials such as polythiophene.

Conclusion

With a WO_3 functionalized CE in parallel and close to the surface of a WE, the reactivity distribution on WE can be successfully projected to the electrochromic CE in the form of local color change, which is then captured by optical imaging. Model systems involving Au interdigitated electrodes, Au microelectrode array, or Au sputtered on ITO as WE, and WO_3 film as CE, are demonstrated. Pure water is used as electrolyte to have high resistance, and the generation of H^+ by oxidation on WE. The latter is essential for driving the coloration of WO_3 CE. The WE is placed in parallel to CE with PTFE spacer controlling the distance. It is seen that the distance needs to be comparable as the size of the target of observation. The effect of voltage and time are studied for inhibiting the lateral color dispersion on CE. This preliminary work opens

the door for mapping the reactivity of WE by the optical change of CE. As the signals are captured from the CE, the method is label-free, that is, does not require specific choice or modification of neither the WE nor the electrolyte. This could be advantageous over optical methods based on direct observation of WE. Possible improvement in both analytical and experimental aspects are discussed.

Acknowledgement

Qiao Liu acknowledges Chinese Scholarship Council for supporting the Ph.D. study. The financial support from LCPME is highly appreciated.

References

[1] K. Ma, Y. Zhang, L. Liu, J. Xi, X. Qiu, T. Guan, Y. He, In situ mapping of activity distribution and oxygen evolution reaction in vanadium flow batteries, Nat. Commun. 10 (2019) 5286. https://doi.org/10.1038/s41467-019-13147-9.

[2] G. Feng, J. Guo, H. Tian, Z. Li, Y. Shi, X. Li, X. Yang, D. Mayerich, Y. Yang, X. Shan, G. Feng, J. Guo, Y. Shi, X. Li, X. Yang, D. Mayerich, X. Shan, H. Tian, Z. Li, Y. Yang, Probe the localized electrochemical environment effects and electrode reaction dynamics for metal batteries using in situ 3D microscopy, Adv. Energy Mater. 12 (2022) 2103484. https://doi.org/10.1002/AENM.202103484.

[3] Y. He, G. Pan, L. Li, S. Zhong, L. Li, Z. Liu, Y. Yu, Local charge transfer within a covalent organic framework and Pt nanoparticles promoting interfacial catalysis, Catal. Sci. Technol. 12 (2022) 3240–3246. https://doi.org/10.1039/D1CY02024B.

[4] A. Almalla, A. Hertwig, D. Fischer, O. Ozcan, J. Witt, Development of layer-by-layer assembled thin coatings on aluminium alloy AA2024-T3 for high resolution

studies of local corrosion processes, J. Appl. Polym. Sci. 137 (2020) 49826. https://doi.org/10.1002/app.49826.

[5] X. Yang, X. Li, S.D. Khochare, P. Ruchhoeft, W.C. Shih, X. Shan, Imaging the electrochemical impedance of single cells via conductive polymer thin film, ACS Sensors. 6 (2020) 485–492. https://doi.org/10.1021/acssensors.0c02051.

[6] D. Polcari, P. Dauphin-Ducharme, J. Mauzeroll, Scanning electrochemical microscopy: A comprehensive review of experimental parameters from 1989 to 2015,116 (2016)13234-13278. https://doi.org/10.1021/acs.chemrev.6b00067.

[7] N. Ebejer, M. Schnippering, A.W. Colburn, M.A. Edwards, P.R. Unwin, Localized high resolution electrochemistry and multifunctional imaging: Scanning electrochemical cell microscopy, Anal. Chem. 82 (2010) 9141–9145. https://doi.org/10.1021/ac102191u.

[8] W. Guo, P. Zhou, L. Sun, H. Ding, B. Su, Microtube electrodes for imaging the electrochemiluminescence layer and deciphering the reaction mechanism, Angew. Chemie. 133 (2021) 2117–2121. https://doi.org/10.1002/ange.202012340.

[9] J.P. Guerrette, S.J. Percival, B. Zhang, Fluorescence coupling for direct imaging of electrocatalytic heterogeneity, J. Am. Chem. Soc. 135 (2013) 855–861. https://doi.org/10.1021/ja310401b.

[10] X. Shan, U. Patel, S. Wang, R. Iglesias, N. Tao, Imaging local electrochemical current via surface plasmon resonance, Science 327 (2010) 1363–1366. https://doi.org/10.1126/science.1186476.

[11] J. Lu, W. Wang, S. Wang, X. Shan, J. Li, N. Tao, Plasmonic-based electrochemical impedance spectroscopy: Application to molecular binding, Anal. Chem. 84 (2012) 21. https://doi.org/10.1021/ac202634h.

[12] Y. Fang, W. Wang, X. Wo, Y. Luo, S. Yin, Y. Wang, X. Shan, N. Tao, Plasmonic imaging of electrochemical oxidation of single nanoparticles, J. Am. Chem. Soc. 136 (2014) 12584–12587. https://doi.org/10.1021/ja507097y.

[13] R. Liu, X. Shan, H. Wang, N. Tao, Plasmonic measurement of electron transfer between a single metal nanoparticle and an electrode through a molecular layer, J. Am. Chem. Soc. 141 (2019) 11694–11699. https://doi.org/10.1021/jacs.9b05388.

[14] Y. Wang, H. Wang, Y. Chen, Y. Wang, H.Y. Chen, X. Shan, N. Tao, Fast electrochemical and plasmonic detection reveals multitime scale conformational gating of electron transfer in Cytochrome c, J. Am. Chem. Soc. 139 (2017) 7244–7249. https://doi.org/10.1021/jacs.7b00839.

[15] D. Jiang, Y. Jiang, Z. Li, T. Liu, X. Wo, Y. Fang, N. Tao, W. Wang, H.Y. Chen, Optical imaging of phase transition and Li-Ion diffusion kinetics of single $LiCoO_2$ nanoparticles during electrochemical cycling, J. Am. Chem. Soc. 139 (2017) 186–192. https://doi.org/10.1021/jacs.6b08923.

[16] J.T. Cao, Y.L. Wang, J.J. Zhang, Y.X. Dong, F.R. Liu, S.W. Ren, Y.M. Liu, Immuno-electrochemiluminescent imaging of a single cell based on functional nanoprobes of heterogeneous $Ru(bpy)_3^{2+}$@SiO_2/Au Nanoparticles, Anal. Chem. 90 (2018) 10334–10339. https://doi.org/10.1021/acs.analchem.8b02141.

[17] Y.M. Long, Q.L. Zhao, Z.L. Zhang, Z.Q. Tian, D.W. Pang, Electrochemical methods – important means for fabrication of fluorescent nanoparticles, Analyst. 137 (2012) 805–815. https://doi.org/10.1039/C2AN15740C.

[18] M.M. Richter, Electrochemiluminescence (ECL), Chem. Rev. 104 (2004) 3003–3036. https://doi.org/10.1021/cr020373d.

[19] Y. Okumura, S. Oana, Effect of counter electrode in electroformation of giant

vesicles, Membranes. 1 (2011) 345–353. https://doi.org/10.3390/membranes1040345.

[20] M.A. Pech-Canul, A.A. Sagüés, P. Castro, Influence of counter electrode positioning on solution resistance in impedance measurements of reinforced concrete, Corrosion. 54 (1998) 663–667. https://doi.org/10.5006/1.3287646.

[21] Y. Wuu, F.F. Fan, A.J. Bard, High Resolution deposition of polyaniline on Pt with the scanning electrochemical microscope, J. Electrochem. Soc. 136 (1989) 885–886. https://doi.org/10.1149/1.2096765.

[22] K.M. Brace, B.E. Hayden, A.E. Russell, J.R. Owen, A parallel optical screen for the rapid combinatorial electrochromic analysis of electrochemical materials, Adv. Mater. 18 (2006) 3253–3257. https://doi.org/10.1002/adma.200600786.

[23] M. Deepa, M. Kar, S.A. Agnihotry, Electrodeposited tungsten oxide films: annealing effects on structure and electrochromic performance, Thin Solid Films. 468 (2004) 32–42. https://doi.org/10.1016/j.tsf.2004.04.056.

[24] M. Mansouri, T. Mahmoodi, Ab initio investigation on the effect of transition metals doping and vacancies in WO_3, Acta Phys. Pol. A. 129 (2016) 8–14. https://doi.org/10.12693/APhysPolA.129.8.

[27] O. Bohnke, B. Vuillemin, Proton insertion into thin films of amorphous WO_3: kinetics study, Mater. Sci. Eng. B. 13 (1992) 243–246. https://doi.org/10.1016/0921-5107(92)90172-6.

[28] Y. Shi, G. Feng, X. Li, X. Yang, A.H. Ghanim, P. Ruchhoeft, D. Jackson, S. Mubeen, X. Shan, Electrochemical impedance imaging on conductive surfaces, Anal. Chem. 93 (2021) 12320–12328. https://doi.org/10.1021/acs.analchem.1c02040.

[29] Y. Wu, B. Zhu, M. Huang, L. Liu, Q. Shi, M. Akbar, C. Chen, J. Wei, J.F. Li, L.R. Zheng, J.S. Kim, H.B. Song, Proton transport enabled by a field-induced metallic state in a semiconductor heterostructure, Science. 369 (2020) 184–188. https://doi.org/10.1126/science.aaz9139.

[30] C.M. Sánchez-Sánchez, J. Rodríguez-López, A.J. Bard, Scanning electrochemical microscopy. 60. quantitative calibration of the SECM substrate generation/tip collection mode and its use for the study of the oxygen reduction mechanism, Anal. Chem. 80 (2008) 3254–3260. https://doi.org/10.1021/ac702453n.

[31] C. Amatore, F. Bonhomme, J.L. Bruneel, L. Servant, L. Thouin, Mapping dynamic concentration profiles with micrometric resolution near an active microscopic surface by confocal resonance Raman microscopy. Application to diffusion near ultramicroelectrodes: first direct evidence for a conproportionation reaction, J. Electroanal. Chem. 484 (2000) 1–17. https://doi.org/10.1016/S0022-0728(00)00057-7.

[32] K. Tu, M.J. Lardner, T.A. Morhart, S.M. Rosendahl, S. Creighton, I.J. Burgess, Spatial Mapping of Methanol Oxidation Activity on a Monolithic Variable-Composition PtNi Alloy Using Synchrotron Infrared Microspectroscopy, J. Phys. reaction, J. Electroanal. Chem. 484 (2000) 1–17. https://doi.org/10.1016/S0022-0728(00)00057-7.